



CZTS thin film solar cells on flexible Molybdenum foil by electrodeposition-annealing route

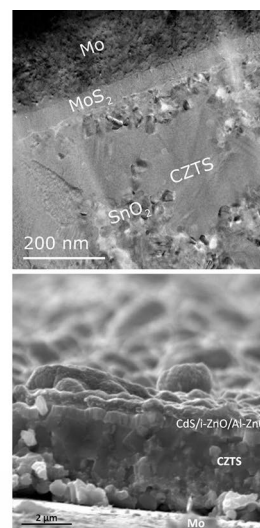
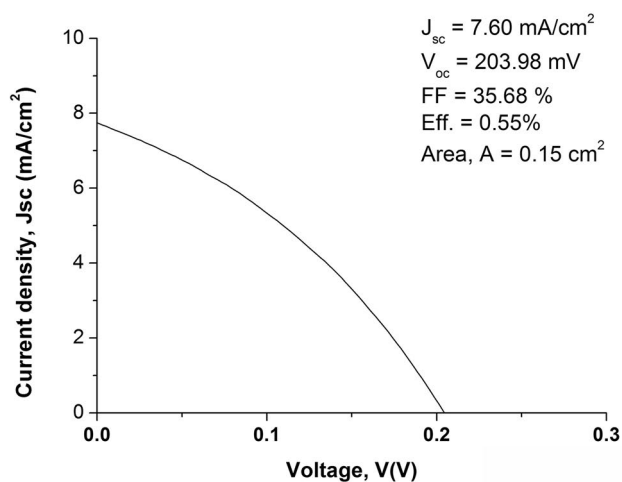
M. I. Khalil¹ · R. Bernasconi¹ · A. Lucotti² · A. Le Donne³ · R. A. Mereu³ · S. Binetti³ · J. L. Hart⁴ · M. L. Taheri⁵ · L. Nobili¹ · L. Magagnin¹

Received: 12 May 2020 / Accepted: 10 October 2020 / Published online: 2 November 2020
© The Author(s) 2020

Abstract

Earth-abundant and non-toxic Kesterite-based $\text{Cu}_2\text{ZnSnS}_4$ (CZTS) thin film solar cells are successfully fabricated on flexible Molybdenum (Mo) foil substrates by an electrodeposition-annealing route. A well-adherent, densely packed, homogeneous, compact, and mirror-like CZT precursor is initially produced through electrodeposition by using a rotating working electrode. Subsequently, the co-electrodeposited CuZnSn (CZT) precursor is sulfurized in quartz tube furnace at 550 °C for 2 h in N_2 atmosphere with the presence of elemental sulfur in order to form CZTS. Different characterization techniques like XRD, SEM, HR-TEM, Raman, and Photoluminescence demonstrate that almost phase-pure CZTS formed after sulfurization. A flexible Al/Al-ZnO/i-ZnO/CdS/CZTS/Mo foil solar cell is produced, where CdS is deposited by chemical bath deposition and transparent conducting oxide (TCO) is deposited by DC sputtering. The CZTS solar device shows a 0.55% power conversion efficiency on flexible Mo foil substrate and it constitutes the first prototype of this kind of solar cell produced by electrodeposition-annealing route without any surface modification of the Mo substrate.

Graphic abstract



Keywords CZTS · Flexible · Molybdenum · Electrodeposition · Sulfurization · Rotating electrode

Electronic supplementary material The online version of this article (<https://doi.org/10.1007/s10800-020-01494-1>) contains supplementary material, which is available to authorized users.

Extended author information available on the last page of the article

1 Introduction

In order to make a real impact on worldwide energy demand (at the TW level), solar materials should be cheap, non-toxic, and earth-abundant, and they should provide high functional lifetime with high power conversion efficiency (PCE). Over the last few decades, thin film technologies based on direct band gap metal chalcogenides have shown the potential to produce photovoltaic (PV) cells with low cost along with easy fabrication routes. Kesterites-based chalcogenides like CZTS ($\text{Cu}_2\text{ZnSnS}_4$), CZTSe ($\text{Cu}_2\text{ZnSnSe}_4$), and mixed sulfo-selenide CZTSSe ($\text{Cu}_2\text{ZnSn}(\text{S}, \text{Se})_4$) are attracting much attention nowadays from researchers as promising alternatives to existing commercialized CIGS ($\text{Cu}(\text{In}, \text{Ga})\text{Se}_2$) and CdTe absorber layers. This is due to the low cost of their mass production, as constituent elements in Kesterites are non-toxic and abundant in the earth's crust compared to CIGS and CdTe. Moreover, they have suitable direct band gap near to 1.45 eV (CZTS), around 1 eV (CZTSe), and 1.0–1.5 eV (CZTSSe, depending on the S/(S + Se) ratio) together with high absorption coefficient ($> 1 \times 10^4 \text{ cm}^{-1}$), which make them ideal among all the second generation thin film solar cells [1–4]. Furthermore, theoretical conversion efficiencies of Kesterites-based solar cells are around 32% like chalcopyrite according to Shockley-Queisser photon balance calculations [5]. Due to the rapid progress of the kesterite material development, the conversion efficiency of the Kesterites-based thin films solar cells have already advanced to 9.4% (CZTS) [6], 11.6% (CZTSe) [7], and 12.6% (CZTSSe) [8]. They are still far behind the theoretical conversion efficiency, despite these remarkable developments.

A suitable fabrication method is important to achieve high-quality Kesterites without having any defects, which ultimately govern the conversion efficiency. The volatile nature of some of their elemental constituents and related binary chalcogenides make the synthesis of stoichiometric Kesterites difficult [9, 10]. In addition, it is difficult to fabricate single-phase Kesterites as they exist within a narrow composition field which is normally known as a Cu-poor ($\text{Cu}/(\text{Zn} + \text{Sn}) \approx 0.7\text{--}0.9$) and Zn-rich ($\text{Zn}/\text{Sn} \approx 1.1\text{--}1.4$) range, according to the phase diagram [9–12]. Besides inappropriate chemical composition of the metallic precursors, binary/ternary chalcogenide phases could also be created due to decomposition of Kesterites at high temperature during sulfurization or selenization [13]. Till now, different vacuum and non-vacuum deposition techniques have been deployed to fabricate Kesterites (CZTS, CZTSe and CZTSSe). Both vacuum and non-vacuum techniques are very much in competition on conversion efficiency, and in some cases, non-vacuum processes are even

more efficient, contrary to the case of CIGS cells where vacuum-based techniques deliver higher conversion efficiencies [8]. Several non-vacuum techniques like sol-gel, electrodeposition, solution-based method etc. have been widely studied to fabricate Kesterites thin films [13–15].

Most of the Kesterites-based thin films solar cells have been fabricated till now on typical Mo-coated soda lime glass (SLG). There are only few reports on fabrication of Kesterites-based solar cells on the flexible substrate like metallic foils or polyimides, irrespective to the fabrication processes [16–24]. Fabrication of Kesterites-based thin film solar cells on the flexible substrate has huge potential in order to minimize production cost due to roll-to-roll manufacturing on the flexible substrate which enables the use of compact size deposition equipment with high throughput [25]. It is, however, important to point out that, in the case of flexible solar cells, efficiency depends on bending radius. Normally, an increase in efficiency for concave bending and a decrease in the case of convex bending is observed [26, 27]. Flexible metal foil substrates like molybdenum (Mo), stainless steel, aluminum (Al), titanium (Ti) etc. are potential candidates of back contact as they are cheap, durable, lightweight, and sustainable at high-temperature sulfurization or selenization processes. In addition to this, a metallic back contact layer is not required when metal substrate is used. On the other hand, the maximum operating temperature of polyimide is typically below 500 °C which makes it unsuitable for those fabrication processes where high-temperature annealing is involved in the presence of sulfur or selenium. Mo foil can be a better choice among all the flexible metallic foil substrates considering its capability to withstand very high temperature along with high conductivity and compatible coefficient of thermal expansion ($5.2 \cdot 10^{-6} \text{ K}^{-1}$) [19]. Moreover, unlike stainless steel, it does not need any diffusion barrier layer to prevent migration of substrate atom during sulfurization or selenization. Till now, maximum power conversion efficiency of CZTS on flexible Mo foil substrate is 3.82% [19], whereas maximum conversion efficiency of CZTS on Mo-coated SLG is 9.4% [6]. On the other hand, maximum power conversion efficiency of CZTS solar cell on flexible stainless steel was reported to be 4.2% through sputtering- H_2S reactive annealing process with the incorporation of alkali doping [18]. CZTS thin film solar cells on Mo foil achieving the efficiency of 3.82% have been fabricated through electrodeposition-annealing route. Point to be noted, before deposition of CZTS on Mo foil, 800 nm Mo back contact was deposited on Mo foil using DC sputtering in their work. Meanwhile, power conversion efficiencies of CZTS and CZTSe on Mo-coated SLG have already reached 8.1% [28] and 8.2% [29], respectively, through electrodeposition-annealing route. It has been demonstrated that alkali doping at the interface of CZTS and Mo has significant effects on the conversion efficiency of the solar cells which

has already been observed in CIGS thin film solar cells [30]. On the other hand, formation of MoS_2 at the interface of CZTS has also substantial effects on conversion efficiency as it is an indirect bandgap semiconductor with a gap of 1.3 eV which creates a back contact blocking (Schottky) barrier that restricts hole transport across the CZTS/Mo interface [31]. Compared to a variety of vacuum-based techniques and wet chemical methods, the material utilization rate in electro-deposition is better than 90%, partly due to the selectivity and partly because there is extensive know-how on the reuse and recycle of electroplating bath [32].

In this work, we fabricated 0.55% efficient CZTS thin film solar cells on flexible Mo foil substrate through electrodeposition-annealing route. Initially, a Cu–Zn–Sn (CZT) precursor is deposited on flexible Mo foil through co-electrodeposition, without sputtering a preliminary Mo layer. Other works reporting precursors deposition on unmodified Mo substrates are available in the literature [33, 34]. The present work, however, presents important elements of innovation and uniqueness. The most important is the approach followed for the deposition step, in which a single alkaline electrolyte is employed to directly deposit CZT. Kalinauskas et al. [33] and Stanchik et al. [34], on the contrary, report CZTS fabrication starting from multilayer precursors of the kind CuSn/Zn or Cu/Zn/Sn, all deposited from acidic electrolytes. Moreover, Stanchik et al. report CZTSe rather than CZTS fabrication. Finally, both Kalinauskas et al. and Stanchik et al. limit the investigation to material fabrication, without producing complete solar cells. Following electrodeposition, the CZT layer is sulfurized at high temperature to get CZTS. Good quality of CZTS depends on the quality of the CZT precursor, and for this reason, high-quality CZT precursor is prepared using rotating working electrode during co-electrodeposition. No sputtering steps are employed on Mo foil before co-electrodeposition of CZT unlike other works in the literature [19]. Following this approach, fabrication process can be considerably simplified and optimized in terms of cost and time.

2 Experimental section

2.1 Electrodeposition of the CZT precursor on Mo foil

Co-electrodeposition of Cu–Zn–Sn (CZT) was carried out under galvanostatic control in a conventional electrochemical cell assembly at room temperature. Formulation of electrolyte bath has already been described in the existing literature [35]. Briefly, such electrolyte contained 2.5 g/l $\text{CuSO}_4 \cdot 5\text{H}_2\text{O}$, 15 g/l $\text{ZnSO}_4 \cdot 7\text{H}_2\text{O}$, 10.5 g/l $\text{Na}_2\text{SnO}_3 \cdot 3\text{H}_2\text{O}$, 200 g/l $\text{K}_4\text{P}_2\text{O}_7$, and 0.4 g/l $\text{CH}_3(\text{CH}_2)_{11}\text{OSO}_3\text{Na}$. A rotating working electrode was used in place of the simple vertical

working electrode (at a rotation speed of 25–35 rpm). Its characteristics are detailed in the supporting materials (figure S1). Flexible Mo foil substrates (200 μm thick, Goodfellow) with an exposed area of $1.6 \times 2.0 \text{ cm}^2$ and titanium mesh were used as a working electrode and counter inert electrode, respectively. Mo substrates were cleaned in acetone, immersed in 32% wt. HCl for 10 min to remove oxide, washed in distilled water, and finally dried under N_2 atmosphere. Mo foil was then mounted on the rotating electrode and the Mo surface was immersed horizontally in the electrolyte. A 30 rpm rotation speed was employed during electrodeposition. Electrodeposition experiments were accomplished by using an AMEL Model-549 Potentiostat. Electrodeposition runs have been performed by using 4.5–5.5 mA/cm^2 current density for 7–8 min, while keeping the pH of the solution at 11. The electrolyte was dummed for 30 min at 5 mA/cm^2 using the same anode/cathode configuration in order to eliminate impurities.

2.2 CZT sulfurization process

After electroplating CZT precursor, the sample was sulfurized at 550 °C for 2 h in a quartz tube furnace with the presence of 25 mg of elemental sulfur powder (Sigma Aldrich; reagent grade, 100 mesh particle size). During sulfurization, a heating rate of 20 °C/minute was used and a very small flow of N_2 was maintained throughout the process [12, 35]. At the end of the process, CZTS was allowed to naturally cooldown.

2.3 CZTS solar cell construction

In order to form the p–n junction, n-type semiconductor CdS ($\approx 70 \text{ nm}$) was deposited by chemical bath deposition on top of CZTS. An 80 nm intrinsic i-ZnO buffer layer, which acts to prevent any shunts, was then deposited by RF sputtering. Later, a TCO layer consisting of 350 nm Al-doped ZnO (AZO) was grown by DC-pulsed (2 kHz) sputtering. Finally, cells were completed by evaporating an Al grid contact on top of it. In this way, Al/Al-ZnO/i-ZnO/CdS/CZTS/Mo foil device has been prepared. 6 single cells, each characterized by a 0.15 cm^2 area, were fabricated on each CZTS coated Mo foil. No anti-reflection coating was used during the measurement of the cells.

2.4 Characterization techniques

Composition, morphology, crystalline phases, and roughness of the CZT precursors and sulfurized CZTS films were investigated by SEM, Laser Profilometry, XRD, SEM, TEM, and Raman spectroscopy. Material band gap was investigated by Photoluminescence (PL) spectroscopy. The formation of impurity and MoS_2 at the interface of CZTS and

Mo was evaluated through HR-TEM and electron energy loss spectroscopy (EELS). The crystallographic phase of sulfurized films was analyzed by X-ray diffraction (XRD), using a Philips X-pert MPD instrument with $\text{CuK}_{\alpha 1}$ radiation (1.5406 Å). The morphology and chemical compositions of the samples were studied by Scanning Electron Microscopy (Model Zeiss EVO 50) together with Energy Dispersive X-ray Spectroscopy (EDS) (Oxford instrument, Model 7060). UBM laser profilometer was used for assessing the roughness parameters. Raman measurements were carried out in the air at room temperature with a micro-Raman spectrometer (Horiba Jobin–Yvon Labram HR800) in the backscattering configuration. The 785 nm excitation wavelength has been used during the Raman characterization of the samples. To avoid the laser heating of the sample, the laser power density was kept as low as possible. The laser power was reduced from 100 to 1 mW at the sample passing through a suitable filtering system with spot size about 1 μm diameter. Here, the beam was focused on the sample using an objective lens with 50 \times magnification. Photoluminescence (PL) spectra of the films have been acquired at 15 K temperature with above bandgap excitation ($\lambda_{\text{exc}} = 805 \text{ nm}$). All PL measurements were performed with a spectral resolution of 6.6 nm using a standard lock-in technique in conjunction with a single grating monochromator and an InGaAs detector. Selected Area Electron Diffraction (SAED) and TEM observation were performed with a JEOL 2100F (Schottky) microscope equipped with a high-resolution pole piece, operated at 200 keV. EELS was acquired with a GIF Quantum and direct-detection sensor with a collection angle of 30 mrad [36]. Solar cell J-V characteristics were taken under Air Mass 1.5 conditions (simulating terrestrial applications) with a Abet Lot-Oriel Solar simulator with the constant incident power density of 1 Sun (100 mW/cm^2) and with Keithley 2440 source meter. Representative data from each characterization technique are reported in the results section.

3 Results and discussion

3.1 CZT deposition on Mo flexible foil

Due to the large reduction potential window among Cu, Zn, and Sn metal ions, it is very difficult to co-electrodeposit CZT from single electrolyte. In our previous work, we were able to electrodeposit them together from single electrolyte where pyrophosphate was used as an only single complexing agent [35]. In order to obtain better precursors in terms of homogeneous distribution of elements and minimum roughness of the film with respect to previous works, here improved bath with rotating working electrode was employed during electrodeposition. It is possible to provide

constant mass flux to the cathode surface using rotating working electrode which is very important to get homogeneous and smooth films. Moreover, it is believed that composition of various elements in the deposited film remains independent of the deposition times when the rotating working electrode is employed during co-electrodeposition [37].

It is well known that Cu-poor, Zn-rich precursor composition is necessary to obtain good kesterite CZTS film due to the narrow composition range for CZTS formation. This happens due to the volatile nature of S, SnS, and Zn during sulfurization which can vary the relative percentage of the elements to a great extent [9, 10, 12] and may result in poor kesterite films, characterized by the extensive formation of secondary phases. For this reason, in this study, Cu-poor and Zn-rich precursor (Cu 43.5 at. %, Zn 33 at. % and Sn 23.5 at. %; $\text{Cu}/(\text{Zn} + \text{Sn}) = 0.77$ and $\text{Zn}/\text{Sn} = 1.4$) has been employed for the fabrication of CZTS. Such CZT composition resulted in quasi-stoichiometric CZTS after annealing [12]. Figure 1 shows the surface morphology and cross-sectional view of the as-deposited CZT film observed by SEM. It is evident that the electrodeposited CZT film is quite homogenous, dense, and continuous, without visible

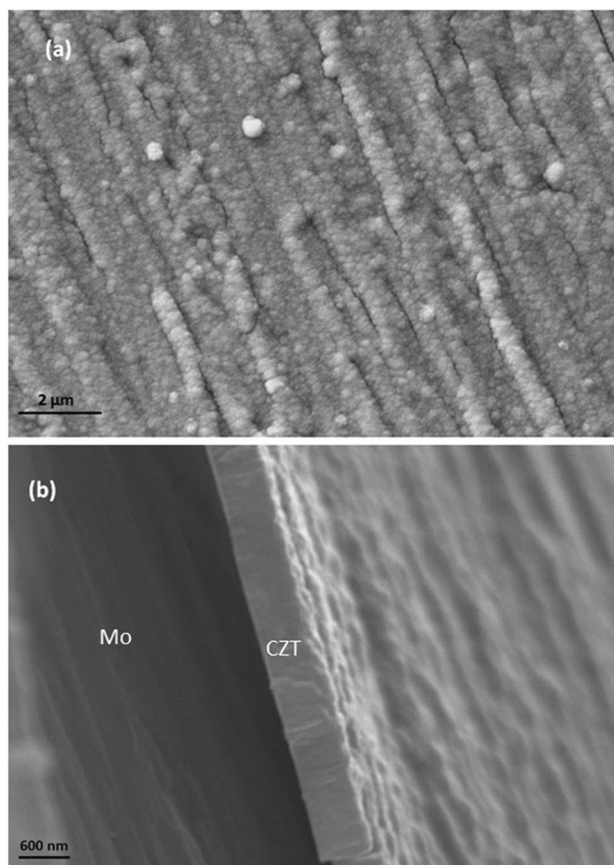


Fig. 1 SEM surface morphology **a** and the cross-sectional view **b** of as-deposited CZT layer

porosity in the cross-section, unlike other results reported in the literature [38]. Moreover, CZT adhesion to the Mo substrate was found to be excellent. Average roughness of the CZT film was around 94 nm, while substrate roughness was around 100 nm, which is quite commendable for the co-electrodeposition of CZT.

3.2 Characterization of sulfurized CZTS on flexible Mo foil

Figure 2a shows the XRD diffractogram of sulfurized kesterite CZTS film. Here, the CZT precursor was sulfurized at 550 °C for 2 h with a heating rate of 20 °C/minute. All the XRD peaks of sulfurized sample correspond to the typical polycrystalline kesterite structure of CZTS (JCPDS card 26–0575) with intense (112) peak at 28.53° which is in agreement with findings of other studies [19, 35, 39–41].

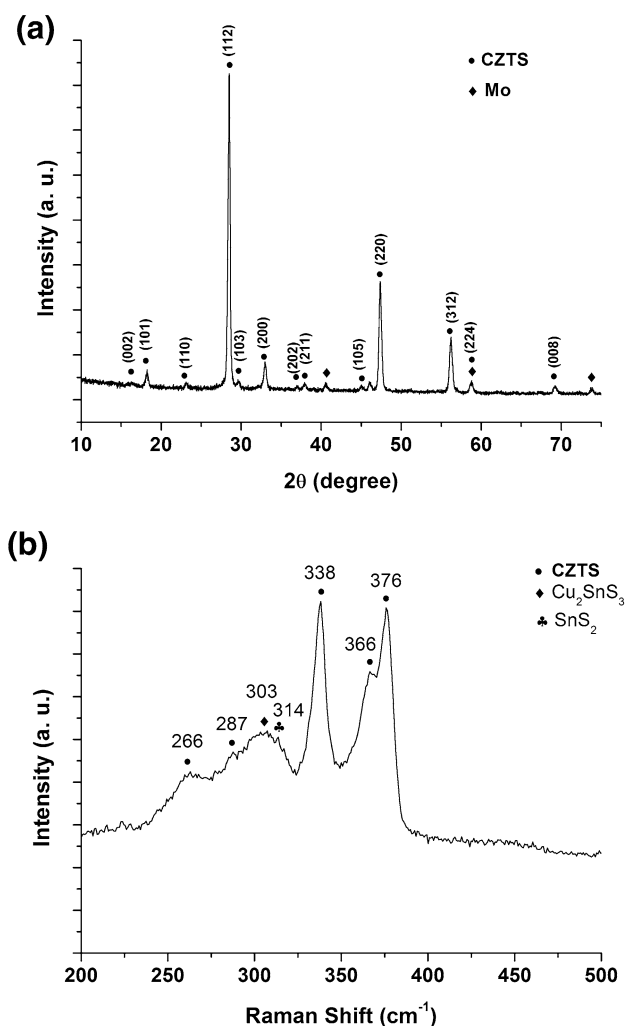


Fig. 2 XRD pattern **a** and Raman spectrum **b** of CZTS film obtained from sulfurization

The sharpness of the diffraction peaks indicates the high crystallinity of the film. Diffraction peaks of CZTS can also be attributed to the ternary phase Cu_2SnS_3 , since they have similar lattice parameters, or to ZnS [42]. As a result, complementary Raman spectroscopy (Fig. 2b) was employed to further characterize the sample. In order to have the better understanding of the formation of CZTS along the film thickness, the 785 nm excitation wavelength has been used. According to previous studies [43], the penetration depth of the 785 nm laser beam in CZTS film is approximately 400 nm and this allows to explore deeper the sample with respect to the 514 nm excitation line with a penetration depth of only 150 nm.

Figure 2b displays the Raman spectrum of the sulfurized CZTS thin film measured at room temperature using the 785 nm excitation wavelength. All the main Raman peaks associated with CZTS were observed at 266 cm^{-1} , 287 cm^{-1} , 338 cm^{-1} , 366 cm^{-1} , and 376 cm^{-1} Raman shift including main intense peak at 338 cm^{-1} which is commonly mentioned in the literature [41, 43–45] and has been associated to the vibration of sulfur atoms [46]. The appearance of two distinct peaks around 367 cm^{-1} and 375 cm^{-1} is typical of Raman spectra of CZTS acquired with excitation laser wavelength of 785 nm [39, 43]. At lower excitation wavelengths, only a broad peak at 367 cm^{-1} is evident. In the Raman spectrum, some additional weaker peaks are also observed at 303 cm^{-1} (cubic Cu_2SnS_3) and 314 cm^{-1} (SnS_2) as reported by other authors [43, 44]. Despite the presence of some secondary phases in film, crystalline CZTS is the largely dominant constituent of the film as the peak intensity of the secondary phases is very weak.

Further insight into the structural properties of the sulfurized CZTS film was gained through high-resolution TEM (HR-TEM) and EELS analysis of a focused ion beam (FIB) prepared using the cross-sectional sample. Figure 3 depicts the HR-TEM of the regions adjacent to the CZTS/Mo interface. TEM imaging and SAED show that the sample is primarily composed of CZTS grains several hundred nm in diameter, in agreement with XRD and Raman results (Fig. 3a and S2). Many twin boundaries and dislocations are visible inside the grains of the CZTS phase, as observed in other studies (Fig. S3 and S4) [47].

The interface between Mo and CZTS was analyzed thoroughly by using HR-TEM and electron energy loss spectroscopy (EELS). In addition to the CZTS, TEM revealed the presence of two secondary phases. As shown in Fig. 3, TEM imaging found a continuous and uniform layer separating the Mo substrate and CZTS film. EELS analysis of this layer shows only Mo and S (Fig. 4b, c), and HR-TEM shows a measured lattice spacing of 6.2 Angstroms (Fig. 3b). Given that the lattice constant of MoS_2 is 6.11 Angstroms, the EELS and HR-TEM data indicate a layer of MoS_2 formed between the Mo substrate and CZTS film. A third phase

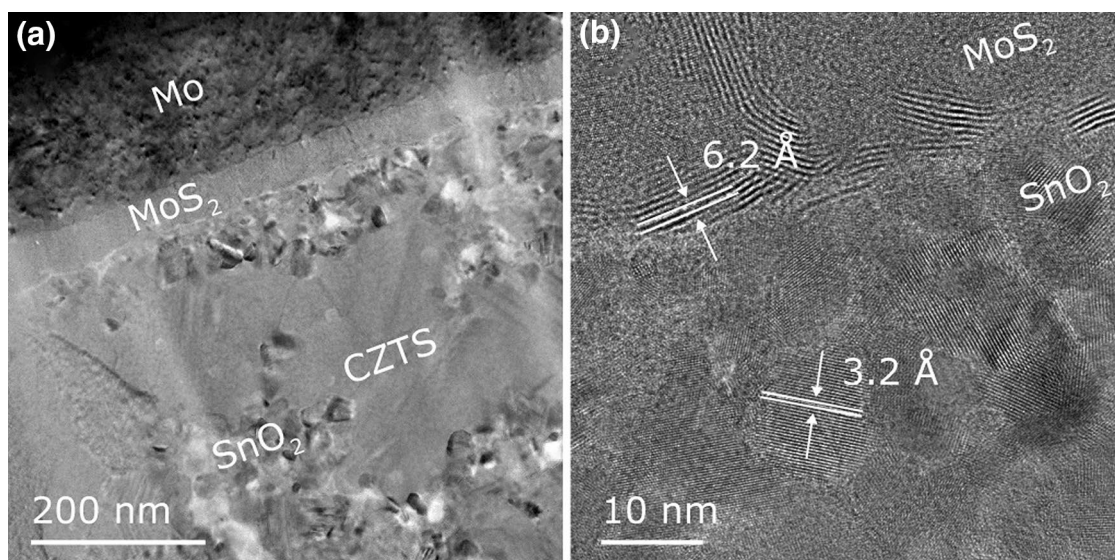


Fig. 3 Low-magnification **a** and high-resolution **b** TEM structural analysis of the interface of CZTS/Mo

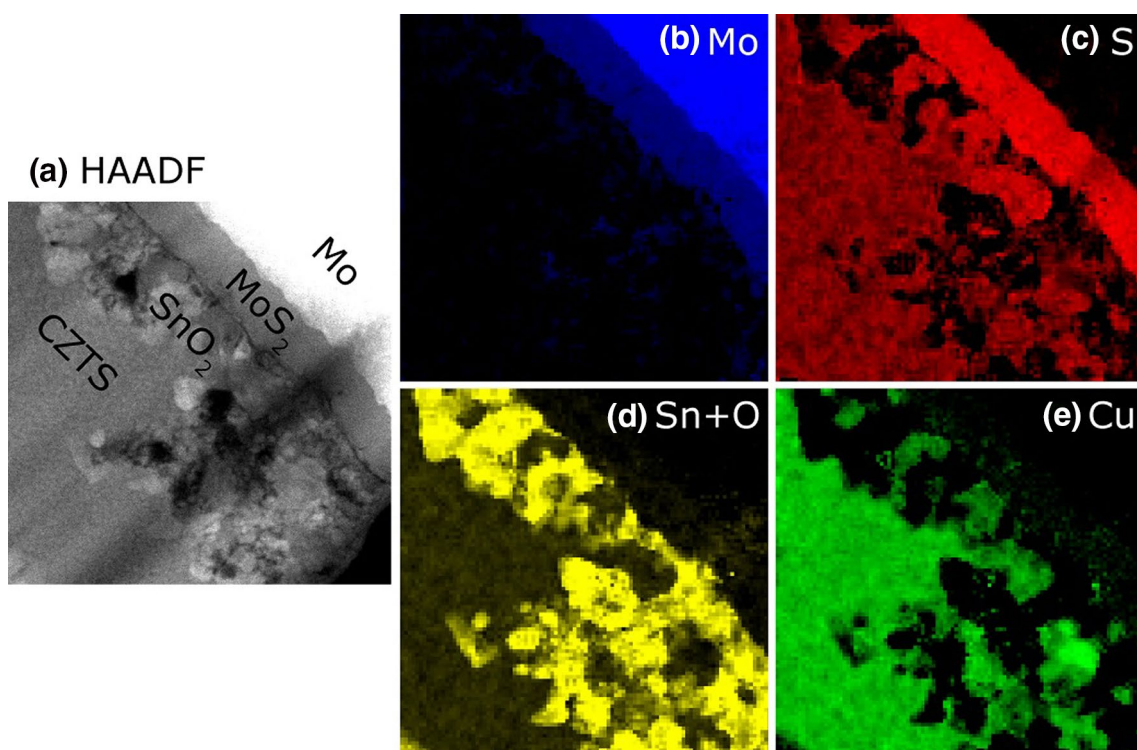


Fig. 4 Electron energy loss spectroscopy (EELS) elemental mapping at the CZTS/Mo interface

is observed in TEM, consisting of nanograin clusters. This phase has a relatively low concentration throughout the CZTS film (Fig. S5 and S6), but the concentration increases considerably near the Mo substrate (Fig. 3a). SAED of this phase is consistent with SnO_2 (Fig. S5). Agreeing with this measurement, EELS shows that this phase only contains Sn

and O (Fig. S6). We note that it is difficult to independently extract the O and Sn EELS signals since the O K edge overlaps the Sn M edge. However, Fig. 4d shows a map of the EELS signal from 470–590 eV, which includes both the O K and Sn M edges. Clearly, there is a large increase in the combined concentration and O + Sn within this third phase,

and Mo, Cu, and S are all absent. By comparing EELS spectra extracted from the CZTS phase and the SnO₂ phase, it is clear that both phases contain Sn, but O is only present within the SnO₂ phase (Fig. S6). The spectra taken from the SnO₂ region closely match those found in the literature [48]. HR-TEM of this phase shows a lattice spacing of 3.2 Angstroms, consistent with the expected value of 3.18 Angstroms for SnO₂.

The presence of MoS₂ and SnO₂ were not detected by XRD or Raman analysis. However, it is possible that these phases were not detected with XRD because of their nanometric size and very low amount. It is also possible that they were located too deep in the CZTS layer to contribute to the Raman signal, provided that their content was above the detection limit of Raman spectroscopy. The source of the SnO₂ clusters is presently unclear; it might be guessed that their formation was caused by the oxidizing impurities of the nitrogen gas used in the sulfurization step. SnO₂ is a large bandgap oxide and a VB offset of approximately 1.5 eV is predicted to exist at the boundary between CZTS and SnO₂; hence this interface might act as a barrier to hole transport [49, 50].

3.3 Complete CZTS solar cell characterization

After the morphological investigation of the formed CZTS layer, complete cells were fabricated. Figure 5 shows the SEM cross-sectional image of the CZTS solar cell, which demonstrates that CZTS possesses bimodal grain distribution where smaller grains are located near the interface with Mo and larger grains at the top of the CZTS.

In order to make sure that fabricated CZTS absorber layers are applicable to photonic devices (i.e., solar cells), samples were further characterized by Photoluminescence Spectroscopy (PL). A typical photoluminescence spectrum of CZTS films at 15 K is reported in Fig. S7, which shows

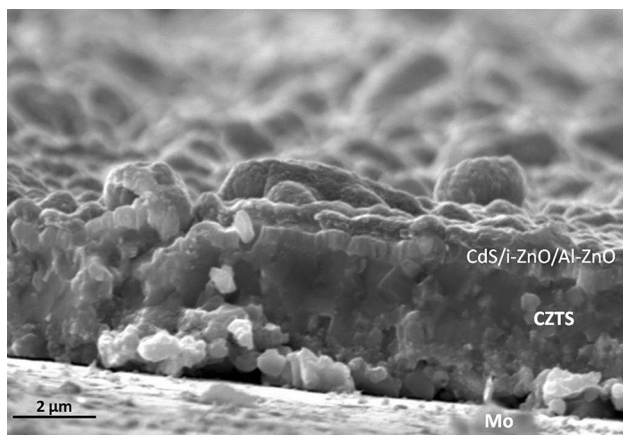


Fig. 5 SEM cross-sectional image of fabricated CZTS solar cell

an asymmetric broad band at 1.21 eV. Similar asymmetric emissions were observed in CZTS fabricated through various methods by different groups [45, 51–53]. According to the literature [51, 52], this band is associated to a quasi-donor–acceptor pair (QDAP) transition, which involves potential fluctuations, as commonly observed in highly defective and compensated semiconductors. It was also demonstrated that the presence of a QDAP emission with saturated peak energy position towards 1.18 eV in the PL spectrum of CZTS layers indicates them as efficient PV absorbers [54].

In order to test the efficiency of the grown layers as PV absorbers, CZTS thin films solar cells were fabricated on Mo foil with classical configuration (Al/Al-ZnO/i-ZnO/CdS/CZTS/Mo foil). Figure 6a shows the current–voltage (J–V) characteristics of CZTS solar cells measured under AM 1.5 illumination. As fabricated Al/Al-ZnO/i-ZnO/CdS/CZTS/Mo foil device shows 0.55% power conversion efficiency

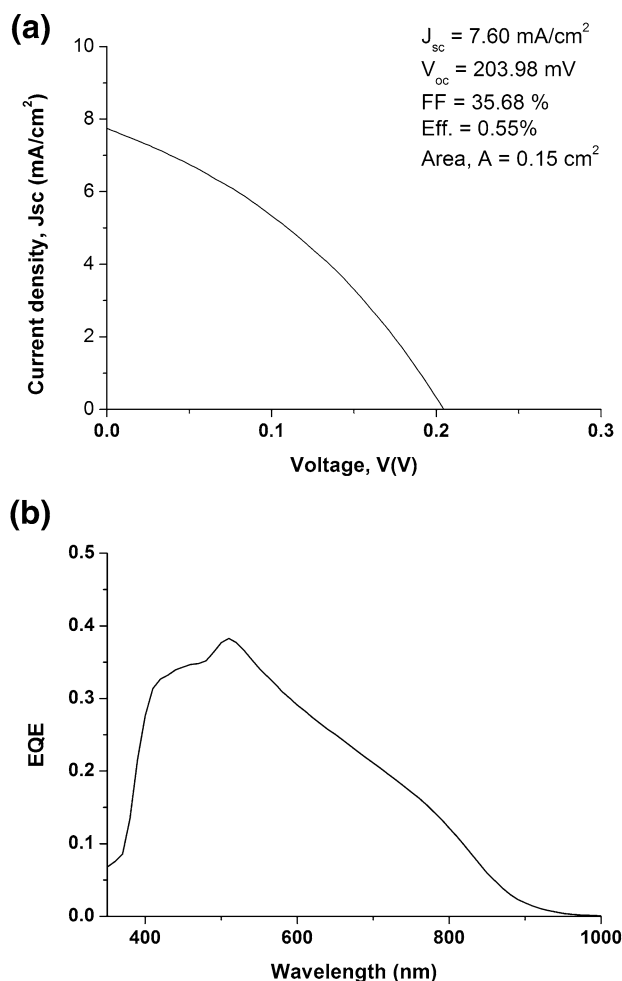


Fig. 6 J–V characteristics of fabricated CZTS solar cell under AM 1.5 illumination (a) and External quantum efficiency (EQE) curve of the CZTS solar cell (b)

(PCE) with $J_{sc} = 7.60 \text{ mA/cm}^2$, $V_{oc} = 203.98 \text{ mV}$ and $FF = 35.68\%$. The low fill factor can come from high series resistance due to back contact electrical characteristics. In addition to this, non-adherence between various layers and morphological problems because of elemental losses during sulfurization can also contribute to lowering both J_{sc} and FF [55]. On the other hand, the small value of V_{oc} is most probably related to the presence of recombination paths may be associated with grain boundaries or other defects. Formation of interfacial MoS_2 during sulfurization process may affect the V_{oc} and alter the band alignment between the CZTS film and MoS_2/Mo . Hence, it may reduce the conversion efficiency of the solar cells since it is in inverse proportion to the solar cell characteristics after the certain limit. It was reported that the formation of MoS_2 interfacial layer at the CZTS/Mo interface enhances the quasi-ohmic electrical contact when it forms with appreciable thickness [56]. On the other hand, a thick MoS_2 layer at the CZTS/Mo interface can influence the total series resistance of the device [41]. However, Zhang et al. recently demonstrated 7.2% efficient CZTS solar cells without having any MoS_2 layer [57]. By the way, HR-TEM suggest around 50 nm of MoS_2 has been formed in our solar cells (Fig. 3). Moreover, the effect of alkali metals (Na, K) on the conversion efficiency of chalcogenide thin film solar cells cannot be ignored, as it has already been reported that alkali incorporation to CIGS increases its open circuit voltage and fill factor [58]. Though the alkali effect on the conversion efficiency was not extensively investigated for CZTS/CZTSe, results similar to those reported for CIGS have been found in case of CZTS also [59, 60]. Alkali incorporation in CZTS can affect the grain size of the final film, the (112) texturing, the free carrier concentration, the hole density and mobility of the film [58]. Yang et al. demonstrated that there is a directly proportional relationship between CZTS thin film solar cells efficiency and Na content in Mo layer. This is probably one of the main reasons why the efficiency of CZTS solar cells on the flexible substrate is far behind that of CZTS solar cells on Mo-coated SLG substrate. Recently Lopez-Marino et al. reported that an improvement in the conversion efficiency of CZTSe solar cells from 2.2% to 4.3% is possible using Mo-Na (Na doped Mo) layer sandwiched between regular Mo layers. After further optimizing the Cr diffusion barrier layer, they reported a record efficiency of 6.1% for a CZTSe solar cell on flexible stainless steel substrate prepared by the sputtering-annealing process [17]. Point to be noted, the device described in the present work is the first prototype of CZTS solar cells on flexible Mo substrate that is realized through electrodeposition-annealing route without any surface modification, to the best of our knowledge.

Figure 6b shows the external quantum efficiency (EQE) spectrum of our CZTS solar cell between 350 and 1000 nm. The EQE demonstrates a low overall spectrum response with

the maximum value of 38.5% (at 510 nm) indicating a high recombination rate, in agreement with V_{oc} value obtained by J-V characterization. The reduction of EQE spectrum in the short wavelength portion is ascribed to the absorption losses in the window and buffer layers (Al-ZnO, i-ZnO, CdS) [41]. On the other hand, recombination processes contribute to lower the EQE values in the long wavelength region.

4 Conclusions

A CZTS thin film solar cell was successfully synthesized on flexible Mo foil substrate by the electrodeposition-annealing method with 0.55% power conversion efficiency. A high-quality CZT precursor without any void or crevice was fabricated by the co-electrodeposition route using rotating working electrode. Formation of MoS_2 at the interface, together with SnO_2 formation near to MoS_2 , can explain the low performances of the final device. Moreover, the absence of alkali metal doping at the substrate can be also associated with such low efficiency of the cell. Nevertheless, first power conversion device based on CZTS thin film solar cell on flexible Mo foil substrate, which has been produced by electrodeposition-annealing route without any surface modification, was demonstrated. In perspective, the good adhesion obtained between the CZTS layer and the Mo substrate constitutes a suitable starting point to perform tests at controlled bending angle and defined number of bending cycles, since it will reasonably prevent active layer delamination. The CZTS cells obtained following the methodology described in the present work constitute, thus, a promising starting point for further process optimization and for additional testing under bending conditions.

Acknowledgements MLT and JLH acknowledge funding in part from the Engineers As Global Leaders for Energy Sustainability EU-Atlantis Program supported by the US Department of Education, and in part from the National Science Foundation's Major Research Instrumentation Program with award #1429661.

Funding Open access funding provided by Politecnico di Milano within the CRUI-CARE Agreement.

Open Access This article is licensed under a Creative Commons Attribution 4.0 International License, which permits use, sharing, adaptation, distribution and reproduction in any medium or format, as long as you give appropriate credit to the original author(s) and the source, provide a link to the Creative Commons licence, and indicate if changes were made. The images or other third party material in this article are included in the article's Creative Commons licence, unless indicated otherwise in a credit line to the material. If material is not included in the article's Creative Commons licence and your intended use is not permitted by statutory regulation or exceeds the permitted use, you will need to obtain permission directly from the copyright holder. To view a copy of this licence, visit <http://creativecommons.org/licenses/by/4.0/>.


References

- Ito K, Nakazawa T (1988) Electrical and optical properties of stannite-type quaternary semiconductor thin films. *Jpn J Appl Phys* 27:2094
- Nakayama N, Ito K (1996) Sprayed films of stannite $\text{Cu}_2\text{ZnSnS}_4$. *Appl Surf Sci* 92:171–175
- Khalate SA, Kate RS, Deokate RJ (2018) A review on energy economics and the recent research and development in energy and the $\text{Cu}_2\text{ZnSnS}_4$ (CZTS) solar cells: A focus towards efficiency. *Sol Energy* 169:616–633
- Pal K, Singh P, Bhaduri A, Thapa KB (2019) Current challenges and future prospects for a highly efficient (> 20%) kesterite CZTS solar cell: A review. *Sol Energy Mater Sol Cells* 196:138–156
- Shockley W, Queisser HJ (1961) Detailed balance limit of efficiency of p-n junction solar cells. *J Appl Phys* 32:510–519
- Tajima S, Umehara M, Hasegawa M et al (2017) $\text{Cu}_2\text{ZnSnS}_4$ photovoltaic cell with improved efficiency fabricated by high-temperature annealing after CdS buffer-layer deposition. *Prog Photovoltaics Res Appl* 25:14–22
- Lee YS, Gershon T, Gunawan O et al (2015) $\text{Cu}_2\text{ZnSnSe}_4$ thin-film solar cells by thermal co-evaporation with 11.6% efficiency and improved minority carrier diffusion length. *Adv Energy Mater* 5(7):1401372
- Wang W, Winkler MT, Gunawan O et al (2014) Device characteristics of CZTSSe thin-film solar cells with 12.6% efficiency. *Adv Energy Mater* 4:1301465
- Scragg JJ, Ericson T, Kubart T et al (2011) Chemical insights into the instability of $\text{Cu}_2\text{ZnSnS}_4$ films during annealing. *Chem Mater* 23:4625–4633
- Redinger A, Berg DM, Dale PJ, Siebentritt S (2011) The consequences of kesterite equilibria for efficient solar cells. *J Am Chem Soc* 133:3320–3323
- Olekseyuk ID, Dudchak IV, Piskach LV (2004) Phase equilibria in the $\text{Cu}_2\text{S}-\text{ZnS}-\text{SnS}_2$ system. *J Alloys Compd* 368:135–143
- Khalil MI, Bernasconi R, Joffe S et al (2015) Effect of co-electrodeposited Cu-Zn-Sn precursor compositions on sulfurized CZTS thin films for solar cell. *ECS Trans* 64:33–41
- Delbos S (2012) Kesterite thin films for photovoltaics: a review. *EPJ Photovoltaics* 3:35004
- Toura H, Khattak YH, Baig F et al (2019) Effect of complexing agent on the morphology and annealing temperature of CZTS kesterite thin films by electrochemical deposition. *Curr Appl Phys* 19:606–613
- Khattak YH, Baig F, Toura H et al (2019) Single step electrochemical deposition for the fabrication of CZTS kesterite thin films for solar cells. *Appl Surf Sci* 497:143794
- López-Marino S, Neuschitzer M, Sánchez Y et al (2014) Earth-abundant absorber based solar cells onto low weight stainless steel substrate. *Sol energy Mater Sol cells* 130:347–353
- López-Marino S, Sánchez Y, Espíndola-Rodríguez M et al (2016) Alkali doping strategies for flexible and light-weight $\text{Cu}_2\text{ZnSnSe}_4$ solar cells. *J Mater Chem A* 4:1895–1907
- Bras P, Sterner J, Platzer-Björkman C (2015) Influence of hydrogen sulfide annealing on copper-zinc-tin-sulfide solar cells sputtered from a quaternary compound target. *Thin Solid Films* 582:233–238
- Zhang Y, Ye Q, Liu J et al (2014) Earth-abundant and low-cost CZTS solar cell on flexible molybdenum foil. *Rsc Adv* 4:23666–23669
- Peng C-Y, Dhakal TP, Garner S et al (2014) Fabrication of $\text{Cu}_2\text{ZnSnS}_4$ solar cell on a flexible glass substrate. *Thin Solid Films* 562:574–577
- Tian Q, Xu X, Han L et al (2012) Hydrophilic $\text{Cu}_2\text{ZnSnS}_4$ nanocrystals for printing flexible, low-cost and environmentally friendly solar cells. *CrystEngComm* 14:3847–3850
- Zhou Z, Wang Y, Xu D, Zhang Y (2010) Fabrication of $\text{Cu}_2\text{ZnSnS}_4$ screen printed layers for solar cells. *Sol Energy Mater Sol Cells* 94:2042–2045
- Khalil MI, Bernasconi R, Pedrazzetti L et al (2017) Co-electrodeposition of metallic precursors for the fabrication of CZTSe thin films solar cells on flexible Mo foil. *J Electrochem Soc* 164:D302–D306
- Sun K, Liu F, Huang J et al (2018) Flexible kesterite $\text{Cu}_2\text{ZnSnS}_4$ solar cells with sodium-doped molybdenum back contacts on stainless steel substrates. *Sol Energy Mater Sol Cells* 182:14–20
- Reinhard P, Chirilă A, Blösch P, et al (2012) Review of progress toward 20% efficiency flexible CIGS solar cells and manufacturing issues of solar modules. In: 2012 IEEE 38th Photovoltaic Specialists Conference (PVSC) PART 2. IEEE, pp 1–9
- Moaven S, Naji L, Taromi FA, Sharif F (2015) Effect of bending deformation on photovoltaic performance of flexible graphene/Ag electrode-based polymer solar cells. *RSC Adv* 5:30889–30901
- Pei L, Yu H, Zhang Q et al (2020) Concave and Convex Bending Influenced Mechanical Stability in Flexible Perovskite Solar Cells. *J Phys Chem C* 124(4):2340–2345
- Jiang F, Ikeda S, Tang Z et al (2015) Impact of alloying duration of an electrodeposited Cu/Sn/Zn metallic stack on properties of $\text{Cu}_2\text{ZnSnS}_4$ absorbers for thin-film solar cells. *Prog Photovoltaics Res Appl* 23:1884–1895
- Vauche L, Risch L, Sánchez Y et al (2016) 8.2% pure selenide kesterite thin-film solar cells from large-area electrodeposited precursors. *Prog Photovoltaics Res Appl* 24:38–51
- Yang K, Sim J, Jeon B et al (2015) Effects of Na and MoS_2 on $\text{Cu}_2\text{ZnSnS}_4$ thin-film solar cell. *Prog Photovoltaics Res Appl* 23:862–873
- Shin B, Zhu Y, Bojarczuk NA et al (2012) Control of an interfacial MoSe_2 layer in $\text{Cu}_2\text{ZnSnSe}_4$ thin film solar cells: 8.9% power conversion efficiency with a TiN diffusion barrier. *Appl Phys Lett* 101:53903
- Deligianni H, Ahmed S, Romankiw LT (2011) The next frontier: electrodeposition for solar cell fabrication. *Electrochem Soc Interface* 20:47
- Kalinauskas P, Norkus E, Mockus Z et al (2020) The Influence of Removal of Secondary Phases and Dissolution By-Product from the Surface of $\text{Cu}_2\text{ZnSnS}_4$ Film on the Photoelectrochemical Response of This Film. *J Electrochem Soc* 167:26513
- Stanchik AV, Gremenok VF, Bashkurov SA et al (2018) Microstructure and Raman scattering of $\text{Cu}_2\text{ZnSnSe}_4$ thin films deposited onto flexible metal substrates. *Semiconductors* 52:215–220
- Khalil MI, Bernasconi R, Magagnin L (2014) CZTS layers for solar cells by an electrodeposition-annealing route. *Electrochim Acta* 145:154–158
- Hart JL, Lang AC, Leff AC et al (2017) Direct detection electron energy-loss spectroscopy: a method to push the limits of resolution and sensitivity. *Sci Rep* 7:1–14
- Colombara D, Crossay A, Vauche L et al (2015) Electrodeposition of kesterite thin films for photovoltaic applications: Quo vadis? *Phys status solidi* 212:88–102
- Kondrotas R, Juškėnas R, Naujokaitis A et al (2015) Characterization of $\text{Cu}_2\text{ZnSnSe}_4$ solar cells prepared from electrochemically co-deposited Cu-Zn-Sn alloy. *Sol energy Mater Sol cells* 132:21–28
- Khalil MI, Atici O, Lucotti A et al (2016) CZTS absorber layer for thin film solar cells from electrodeposited metallic stacked precursors (Zn/Cu-Sn). *Appl Surf Sci* 379:91–97
- Marchionna S, Garattini P, Le Donne A et al (2013) $\text{Cu}_2\text{ZnSnS}_4$ solar cells grown by sulphurisation of sputtered metal precursors. *Thin Solid Films* 542:114–118

41. Ahmed S, Reuter KB, Gunawan O et al (2012) A high efficiency electrodeposited Cu₂ZnSnS₄ solar cell. *Adv Energy Mater* 2:253–259
42. Walsh A, Chen S, Wei S, Gong X (2012) Kesterite thin-film solar cells: Advances in materials modelling of Cu₂ZnSnS₄. *Adv Energy Mater* 2:400–409
43. Fernandes PA, Salomé PMP, Da Cunha AF (2011) Study of polycrystalline Cu₂ZnSnS₄ films by Raman scattering. *J Alloys Compd* 509:7600–7606
44. Lin X, Kavalakkatt J, Kornhuber K et al (2013) Structural and optical properties of Cu₂ZnSnS₄ thin film absorbers from ZnS and Cu₃SnS₄ nanoparticle precursors. *Thin Solid Films* 535:10–13
45. Altosaar M, Raudoja J, Timmo K et al (2008) Cu₂Zn_{1-x}Cd_xSn (Se_{1-y}S_y) 4 solid solutions as absorber materials for solar cells. *Phys status solidi* 205:167–170
46. Himmrich M, Haeuseler H (1991) Far infrared studies on stannite and wurtzstannite type compounds. *Spectrochim Acta Part A Mol Spectrosc* 47:933–942
47. Kattan N, Hou B, Fermín DJ, Cherns D (2015) Crystal structure and defects visualization of Cu₂ZnSnS₄ nanoparticles employing transmission electron microscopy and electron diffraction. *Appl Mater Today* 1:52–59
48. Lorenz H, Zhao Q, Turner S et al (2010) Preparation and structural characterization of SnO₂ and GeO₂ methanol steam reforming thin film model catalysts by (HR) TEM. *Mater Chem Phys* 122:623–629
49. Ge J, Yu Y, Ke W et al (2016) Improved Performance of Electroplated CZTS Thin-Film Solar Cells with Bifacial Configuration. *Chemosuschem* 9:2149–2158
50. Kim JH, Choi S, Choi M et al (2016) Atomic-scale observation of oxygen substitution and its correlation with hole-transport barriers in Cu₂ZnSnSe₄ thin-film solar cells. *Adv Energy Mater* 6:1501902
51. Le Donne A, Marchionna S, Garattini P, et al (2015) Effects of CdS buffer layers on photoluminescence properties of Cu₂ZnSnS₄ solar cells. *Int J Photoenergy* 2015:
52. Leitão JP, Santos NM, Fernandes PA et al (2011) Study of optical and structural properties of Cu₂ZnSnS₄ thin films. *Thin Solid Films* 519:7390–7393
53. Tanaka K, Miyamoto Y, Uchiki H et al (2006) Donor-acceptor pair recombination luminescence from Cu₂ZnSnS₄ bulk single crystals. *Phys status solidi* 203:2891–2896
54. Gershon T, Shin B, Gokmen T et al (2013) Relationship between Cu₂ZnSnS₄ quasi donor-acceptor pair density and solar cell efficiency. *Appl Phys Lett* 103:193903
55. Vauche L, Dubois J, Laparre A et al (2015) Rapid thermal processing annealing challenges for large scale Cu₂ZnSnS₄ thin films. *Phys Status Solidi* 212:103–108
56. Habas SE, Platt HAS, Van Hest MFAM, Ginley DS (2010) Low-cost inorganic solar cells: from ink to printed device. *Chem Rev* 110:6571–6594
57. Zhang Z, Yao L, Zhang Y et al (2018) Modified back contact interface of CZTSe thin film solar cells: elimination of double layer distribution in absorber layer. *Adv Sci* 5:1700645
58. Salomé PMP, Rodriguez-Alvarez H, Sadewasser S (2015) Incorporation of alkali metals in chalcogenide solar cells. *Sol Energy Mater Sol Cells* 143:9–20
59. Oo WMH, Johnson JL, Bhatia A et al (2011) Grain size and texture of Cu₂ZnSnS₄ thin films synthesized by cosputtering binary sulfides and annealing: effects of processing conditions and sodium. *J Electron Mater* 40:2214
60. Prabhakar T, Jampana N (2011) Effect of sodium diffusion on the structural and electrical properties of Cu₂ZnSnS₄ thin films. *Sol Energy Mater Sol Cells* 95:1001–1004

Publisher's Note Springer Nature remains neutral with regard to jurisdictional claims in published maps and institutional affiliations.

Affiliations

M. I. Khalil¹ · R. Bernasconi¹  · A. Lucotti² · A. Le Donne³ · R. A. Mereu³ · S. Binetti³ · J. L. Hart⁴ · M. L. Taheri⁵ · L. Nobili¹ · L. Magagnin¹

✉ L. Magagnin
luca.magagnin@polimi.it

¹ Department of Chemistry, Materials and Chemical Engineering “Giulio Natta”, Politecnico Di Milano, Via Mancinelli 7, 20131 Milano, Italy

² Department of Chemistry, Materials and Chemical Engineering “Giulio Natta”, Politecnico Di Milano, Piazza Leonardo da Vinci 32, 20133 Milano, Italy

³ Department of Materials Science and Solar Energy Research Centre (MIB-SOLAR), University of Milano - Bicocca, Via Cozzi 55, 20125 Milano, Italy

⁴ Department of Materials Science and Engineering, Drexel University, Philadelphia, PA, USA

⁵ Department of Materials Science and Engineering, Johns Hopkins University, Baltimore, MD 21218, USA